W. Raab, A. Poglitsch, R. Klein, R. Hoenle, M. Schweizer, W. Viehhauser, N. Geis, R. Genzel, L. W. Looney, M. Hamidouche, T. Henning and E. E. Haller, "Characterizing the system performance of FIFI LS: the field-imaging far-infrared line spectrometer for SOFIA", Proc. SPIE 6269, 62691G (2006).

http://dx.doi.org/10.1117/12.671483

Characterizing the system performance of FIFI LS: the field-imaging far-infrared line spectrometer for SOFIA

W. Raab[a], A. Poglitsch[a], R. Klein[b], R. Hoenle[a], M. Schweizer[a], W. Viehhauser[a], N. Geis[a], R. Genzel[a], L. W. Looney[c], M. Hamidouche[c], T. Henning[d] and E.E. Haller[b]

[a]Max-Planck-Institut für extraterrestrische Physik, Garching, Germany;
[b]University of California, Berkeley, USA;
[c]University of Illinois, Urbana-Champaign, USA;
[d]Max-Planck-Institut für Astronomie, Heidelberg, Germany

ABSTRACT

FIFI LS is a Field-Imaging Line Spectrometer designed for the SOFIA airborne observatory. The instrument will operate in the far infrared wavelength range between 42 to 210 microns. Two spectrometer bands from 42 - 110 microns ('blue' channel) and 110 - 210 microns ('red' channel) allow simultaneous and independent diffraction limited 3D imaging over a field of view of 6 x 6 and 12 x 12 arcseconds respectively. Both spectrometer channels use Littrow mounted diffraction gratings, a set of anamorphic collimators, and a reflective integral field unit. Two large scale 25 x 16 pixel Ge:Ga detector arrays are utilized, axially stressed in the red channel and only slightly stressed in the blue channel. The spectral resolution of the instrument varies between R = 1400 to 6500 depending on wavelength. The sensitivity of the instrument will allow background limited performance over the entire wavelength range. We present test results for the components in the optical path of FIFI LS including grating efficiencies, filter characteristics, detector performance, and optical throughput. Based on our measurements we characterized and optimized the overall system performance to maximize observing efficiency - one of the major instrument design criteria.

Keywords: Integral Field Imaging, Spectrometer, Far-Infrared, FIFI, FIFI LS, SOFIA

1. INTRODUCTION

Modern astronomy relies heavily upon so called 3D-imaging to investigate the morphology and dynamics of extended structures. This technique allows to obtain both spectral (radial velocity) and spatial (the field of view) information simultaneously. Besides its obvious strength of obtaining a complete datacube in one single observation, the 3D imaging technique also produces highly reliable datasets due to the parallel and simultaneous data acquisition.

The Far-Infrared Field-Imaging Line Spectrometer (FIFI LS[1–5]) is a 3D-imaging spectrometer designed and built at the MPE-Garching for the Stratospheric Observatory for Infrared Astronomy (SOFIA). FIFI LS will allow 3-dimensional imaging in two nearly independent far-infrared wavelength bands: 42 to 110 μm and 110 to 210 μm, over a field of view of 6 x 6 arceseconds in the short and 12 x 12 arcseconds in the long waveband respectively. Depending on wavelength each observation covers a spectral range of 400 to 1700 km/s at a spectral resolution of R =1400 - 6500.

The integration of FIFI LS at the MPE-Garching is drawing to a close. The long wavelength spectrometer is fully equipped and in flight-ready configuration. All components of the short wavelength spectrometer are in house and will be integrated right after the initial test phase of the red spectrometer. The entire warm read-out electronics is assembled and operational. A series of instrument cool downs has been performed during spring 2006 to verify that FIFI LS is reaching the specifications proposed in the design phase. In this paper we present results of these initial instrument tests as well as test results of individual instrument components.

Further author information: (Send correspondence to W.R.)
E-mail: raab@mpe.mpg.de, http://fifi-ls.mpe.mpg.de

Ground-based and Airborne Instrumentation for Astronomy, edited by Ian S. McLean, Masanori Iye,
Proc. of SPIE Vol. 6269, 62691G, (2006) · 0277-786X/06/$15 · doi: 10.1117/12.671483

2. INSTRUMENT OVERVIEW

The instrument is discussed in detail elsewhere in this volume,[6] so only a brief description of the overall system is given here.

2.1. Cryostat

In order to minimize the infrared background, the optical components of FIFI LS need to be cooled to at least 4.5K. The detector arrays (see section 2.3) require an even lower operating temperature of ∼1.7K (stressed array) and ∼2.5K (unstressed array) respectively. The FIFI LS cryostat therefore requires liquid Helium to cool the components of the spectrometers, and pumped liquid Helium for cooling the detector arrays. An additional temperature stage cooled by liquid Nitrogen is required to minimize the radiative heat load onto the liquid Helium area. The FIFI LS cryostat therefore contains three cryogen containers: A ∼32 liter liquid Nitrogen vessel, A 35 liter liquid Helium vessel, and an additional ∼3.12 liter liquid Helium container, that can be pumped to reach the required operating temperature of the detector arrays.

An adjustable dichroic beam splitter is mounted near the entrance window of the cryostat to separate the light from the telescope around the cut off wavelength of ∼ 2 μm. The short wavelength radiation transmitted by the dichroic is used for guiding of the telescope, while the mid and far infrared radiation is reflected into the cryostat through a thin polyethylene window (see section 3.1.2).

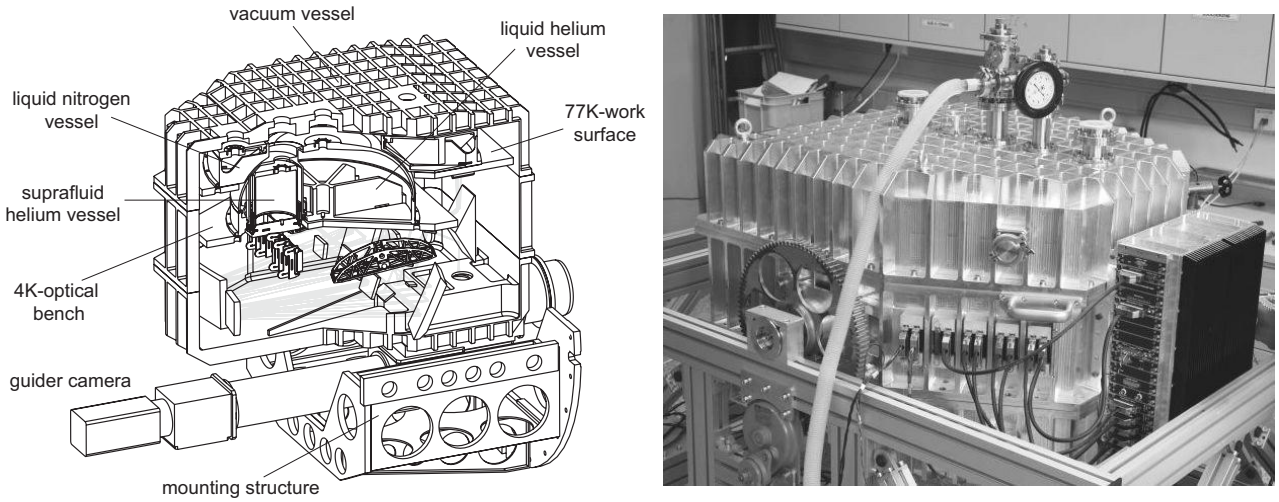

Figure 1. A schematic cut through the FIFI LS cryostat (left) and a picture of the actual instrument in the laboratory during a cool down (right).

2.2. Optics Design

Although a detailed discussion of the optical design of FIFI LS can be found in another volume of the Proceedings of SPIE,[5] we will briefly review the overall optical system here. As mentioned above, FIFI LS is a two channel spectrometer that allows simultaneous observations in the wavelength bands 42 - 110 μm and 110 - 210 μm. The two spectrometer channels share a common entrance optics, which is used for image de-rotation as well as re-focusing of the light onto the slicer mirrors. The entrance optics and a chopped dual-temperature calibration source are mounted in the liquid nitrogen area of the instrument. The two otherwise independent spectrometers are separated right after entering the liquid helium area at the Lyot-stop by exchangeable multi layer interference dichroics (see section 3.1.1). The only difference in both spectrometer bands is a set of re-imaging mirrors that

doubles the image size on the blue image slicer resulting in a close to diffraction limited pixel size of 12 arcseconds in the long wavelength and 6 arcsecond in the short wavelength spectrometer.

An image slicer system in each wavelength band rearranges the two dimensional 5×5 pixel field of view along a one dimensional pseudo slit, forming the entrance slit to the grating spectrometer. Littrow mounted diffraction gratings optimized for the respective waveband are used for spectral multiplexing in each spectrometer band. The grating in the red spectrometer, covering less than an octave in wavelength, is operated in first diffraction order only. The blue grating has to be operated in first and second order to fully cover the blue wavelength band. The calculated efficiency of the red grating peaks at 148 μm reaching an efficiency of ∼98%, while the blue grating, optimized for two diffraction orders, only reaches a peak efficiency of around 75% at 55 μm (1st order) and 90 μm (2nd order) respectively.

After returning from the Littrow spectrometers, the spectra are re-imaged onto the detector arrays by anamorphic exit optics with the appropriate magnification in the 'spectral' and 'spatial' dimension. Light cones attached in front of the individual pixel provide area filling coverage of the focal plane.

2.3. Detector Arrays

As mentioned above, FIFI LS will uses two detector arrays to cover the wavelength range between 42 - 110 μm and 110 - 210 μm. For both arrays we use Gallium doped Germanium (Ge:Ga) photoconductors, which offer high sensitivity up to 120 μm. Application of mechanical stress of 600 - 700 N/mm^2 shifts the wavelength response of the detector material to almost 220 μm. Accordingly we use two large format 16×25 pixel Ge:Ga detector arrays:[7–9] a high stress array in the long wavelength spectrometer and a low stress (∼100 N/mm^2) array in the short wavelength spectrometer.

The mechanical assembly of both arrays is very similar. Each array is made of 25 individual modules containing a stack of 16 stressed pixels. The main body of each module is designed as a spring mechanism keeping the stress constant after cool down. Mechanical stress is applied by a stressing screw at the top of the module. Careful mechanical design provides de-coupling of the housing and the pixel stack to prevent buckling of the stack. The pixels are mounted inside a gold metallized integrating cavity to increase the quantum efficiency. To provide area filling light collection, a light cone module is mounted in front of each detector module. All high stress modules plus spares, as well as nine low stress modules have been assembled to date. We plan to finish the integration of the remaining low stress modules by the end of the year.

2.4. Read-out Electronics

An active cold read-out electronic circuit (CRE)[10] is located at the back end of each detector module. The CRE is based on CMOS technology and was developed by IMEC, Leuven/Belgium for the Herschel-PACS[11] instrument. The CRE is a Capacitive Feedback Transimpedance Amplifier (CTIA) containing 18 (16 + 2 dummies) current integrators with a sample-and-hold stage and a multiplexer. Four different values for the integrating capacitor can be selected. The open loop gain of the input stage is of order 1000. The CRE design allows destructive (with capacitor reset) as well as non-destructive (without capacitor reset, 'sampling up the ramp') read-out. The CRE circuit is mounted on a ceramic substrate containing passive elements to provide stable bias voltages. The non-destructive frame rate is 256 Hz, with the multiplexer running at 8192 Hz. Typical reset intervals (destructive read-out) are 0.125 - 1 s. The CRE are designed to operate at a temperature of 4K and below. The power dissipation of a complete CRE module is around 100 μW leading to a total power consumption of 2.5 mW for an entire 25 module detector array.

3. INSTRUMENT PERFORMANCE

The performance of each component of FIFI LS was verified after delivery or manufacture. We used a Fourier transform spectrometer (FTS) to verify our filters, gratings, and other optical components. Measurements at ASTEQ in Kelkheim/Germany were used to characterize the response curve of the detector modules as a function of wavelength. In addition, a series of cool downs with the long wavelength spectrometer in flight configuration were carried out to determine the overall system performance of the instrument. The following sections summarize the results of these measurements.

3.1. Optical Components

3.1.1. Filters and Dichroics

The optical system of FIFI LS includes a number of multi layer interference filters manufactured by Cardiff University, Cardiff/UK. Table 1 summarizes the optical and physical properties of all filters and dichroics used in the instrument.

Table 1. Properties of the filters used in FIFI LS.

Filter	Type	Position	Blocking λ	Transmitting λ	Diameter
FL2	low pass	Lyot stop	0 - 48 μm	$\sim$51 - >210 μm	22 mm
FRO1	low pass	red pupil	0 - 100 μm	100 - >220 μm	15 mm
FBO1	band pass	blue pupil	bandpass	72 - 130 μm	15 mm
FBO2	band pass	blue pupil	bandpass	50 - 72 μm	15 mm
D1	dichroic	dichroic changer	41 - 105 μm	105 - 220 μm	25 mm
D2	dichroic	dichroic changer	60 - 130 μm	130 - 220 μm	25 mm

All filters are purchased, delivered and fully characterized by measurement of transmissivity and reflectivity (for dichroics). Fig. 2 show typical results of these measurement for filter FL2 (filter #1155) and dichroic D2 (filter #1465). We have found some degree of 'fringing' occurring in the transmissivity of all our filters resulting from the multi-layer structure of the filters. Most of our filters also show a moderate amount of 'leakage' at wavenumbers between 310 and 350 cm^{-1}. This behavior will not be much of a problem, since we will use at least two filters with leakage at different wavelength in each spectrometer band. The only potential problem is the non-ideal behavior of the reflectivity of our dichroics at high wavenumbers. This will lead to a certain degree of light loss and as a consequence a small decrease of sensitivity in the short wavelength band.

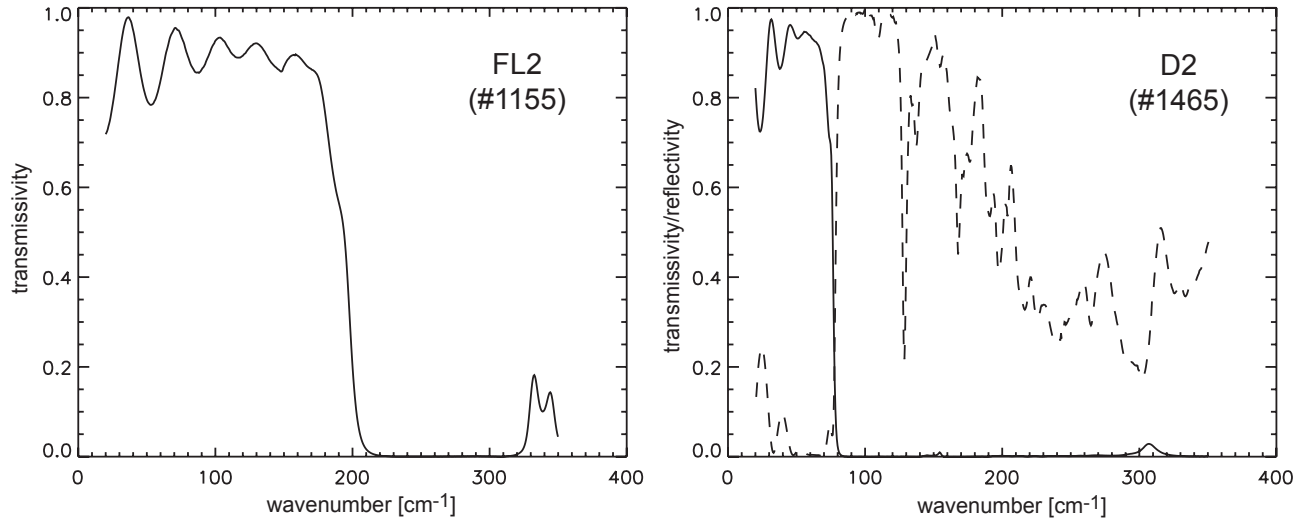

Figure 2. Typical filter curves of filters used in FIFI LS (compare Table 1). Left: Transmissivity of filter FL2. Right: Transmissivity and reflectivity of dichroic D2. Transmissivities are shown in solid lines, reflectivities in dashed lines.

3.1.2. Cryostat Window

The cryostat window of FIFI LS has a diameter of 40 mm and is made of thin (40 - 75 μm), bi-directionally stretched polypropylene. The properties of the cryostat window show significant impact on the instrument performance by two main mechanism: (1) the window adds to the general infrared background since it is mounted

at room temperature and shows significant emissivity and (2) because the thickness of the material is in the order of the observing wavelength there is a wavelength dependent 'fringing' in the transmissivity of the window. Fig. 3 shows the measured transmissivity of two polypropylene foil samples with a thickness of 40 μm and 50 μm respectively. Both samples reach a maximum transmissivity of close to 100% and at least 84% over the entire wavelength range of FIFI LS. The main difference is the exact location of the peak transmission. Unfortunately it is not possible to find a window that shows high transmissivity at all main astronomical FIR emission lines (compare transmission values for 63 μm and 158 μm). We will therefore prepare at least two windows optimized for the respective astronomical 'lines of interest' that can be exchanged in between flights series.

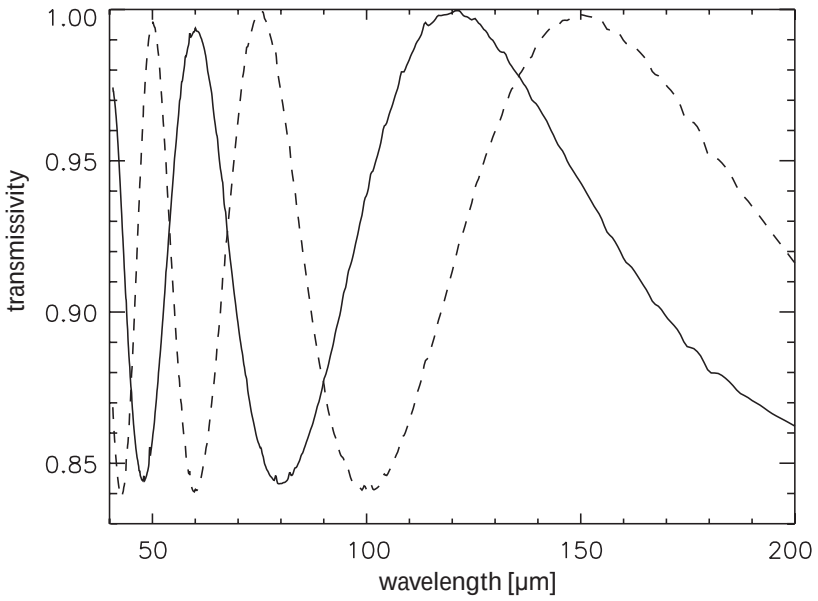

Figure 3. Transmission curves for 40 μm (solid line) and 50 μm (dashed line) polypropylene foil used as window material for FIFI LS.

3.1.3. Diffraction Gratings

Both gratings used in FIFI LS are machined by diamond milling. The physical parameters of the gratings are listed in Table 2. The grating for the short wavelength spectrometer was manufactured in acceptable quality by Hyperfine, Boulder/Colorado, while the technically much more challenging long wavelength grating was manufactured by Zumtobel Staff in Dornbirn/Austria. Both gratings meet our specifications, verified by a 10μm interferogram in case of the short wavelength grating and by comparison of the measured and theoretical efficiency curve for the long wavelength grating.

Table 2. Properties of the two diffraction gratings used in FIFI LS.

	long wavelength	short wavelength
groove density	8.5/mm	12.0/cm
# of grooves, total	∼2720	∼3840
groove period	117.65μm	83.3μm
enclosed angle	44°	84°
groove depth	140μm	42.5μm

Fig. 4 shows the measured and calculated efficiency curve for the long wavelength grating in 0^{th} order. The measurement was performed using a Fourier transform spectrometer (FTS) with an angle of 19° between incident and diffracted beam. Due to alignment problems in our setup, the efficiency of other than 0^{th} orders is extremely hard to measure and are therefore - although in agreement with the theoretical predictions - not considered very reliable. The calculation has been performed using PCGrate-1E Vers. 3.0, which allows numerically solving Maxwell's equations with periodic boundary conditions. In general we observe a very good agreement between the measured efficiency and the theoretical prediction leading us to the conclusion that the general parameters of the grating do not deviate much from the specified values. The calculation also showed, that the exact values of the efficiency curve strongly depend on the polarization of the beam. The calculated efficiency curve shown in Fig. 4 assumes completely unpolarized light. The deviation in the region between 100 - 160 μm most probably is due to a certain degree of polarization of the beam in the FTS.

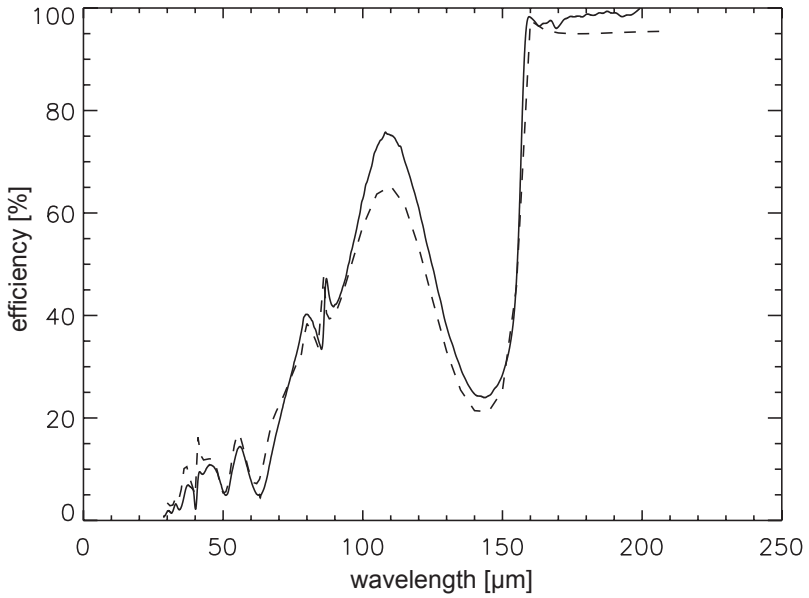

Figure 4. Measured and calculated efficiency curve of the long wavelength grating in 0^{th} order. The solid line shows the measurement, the dashed line the result of a calculation using PCGrate.

3.2. Detector Performance

A series of cool downs has been used to investigate the performance of the detectors. We have produced a 'mixed' detector array composed of high stress and low stress modules to get the full information about both types of detectors in a single cool down. The mixed array was placed in the fully equipped long wavelength spectrometer of FIFI LS.

3.2.1. Responsivity and Cut-off Wavelength

Spectral response curves have been produced by ASTEQ, Kelkheim/Germany. Fig. 5 show typical response curves of pixels in low stress and a high stress modules. The measurement was performed at 100 mV bias for the low stress and 40 mV bias for the high stress module. The curves were used to determine the cut-off wavelength defined by a 50% drop of the spectral response. We calculate a cut-off wavelength of 141 μm for the low stress and 197 μm for the high stress modules. The cut-off wavelength of individual pixels in one detector module differ by less than 5%, demonstrating the stress homogeneity achieved.

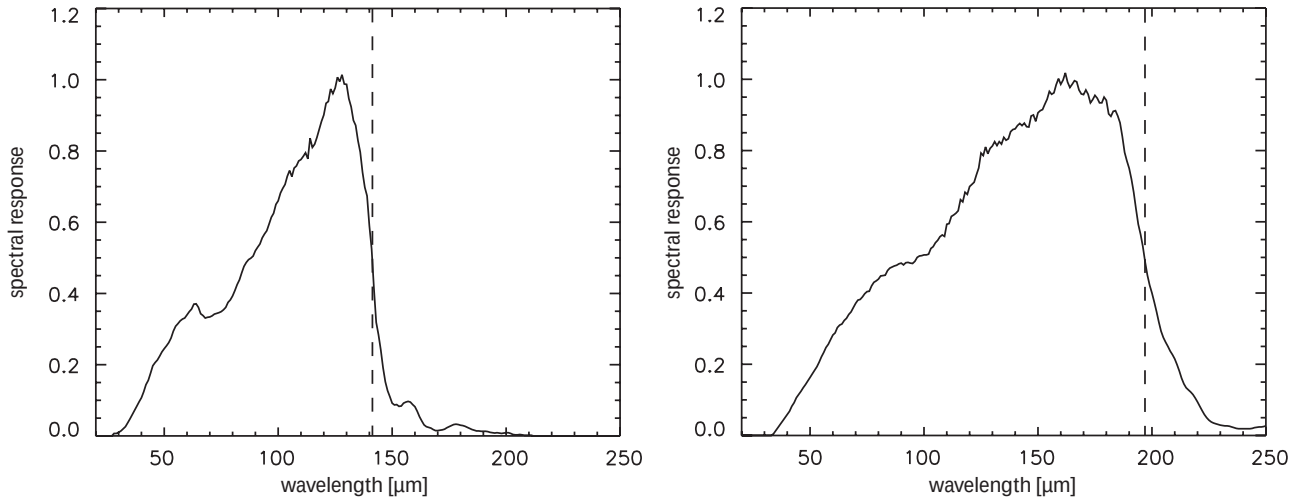

Figure 5. Typical relative spectral response of a low stress (left) and high stress (right) detector pixel. The peak response both curves is normalized individually. The dashed vertical lines mark the wavelengths of 50% response decrease, defining the cut-off wavelength.

3.2.2. Noise Performance

The signal of an internal blackbody source of known temperature was used to analyze the noise performance of the stressed detectors. The left panel of Fig. 6 shows five typical integration ramps measured at a blackbody temperature of 35 K and a bias voltage of 40 mV. On the right panel we show one of the ramps after subtraction of the average ramp slope, illustrating the noise on the integration ramps. From these measurements we calculate a signal to noise ratio of at least 1200 and a detector NEP of better than $1.2 \times 10^{-16}\ W/\sqrt{Hz}$. It should be noted that these values are still preliminary and a more detailed analysis of the detector noise performance will have to follow.

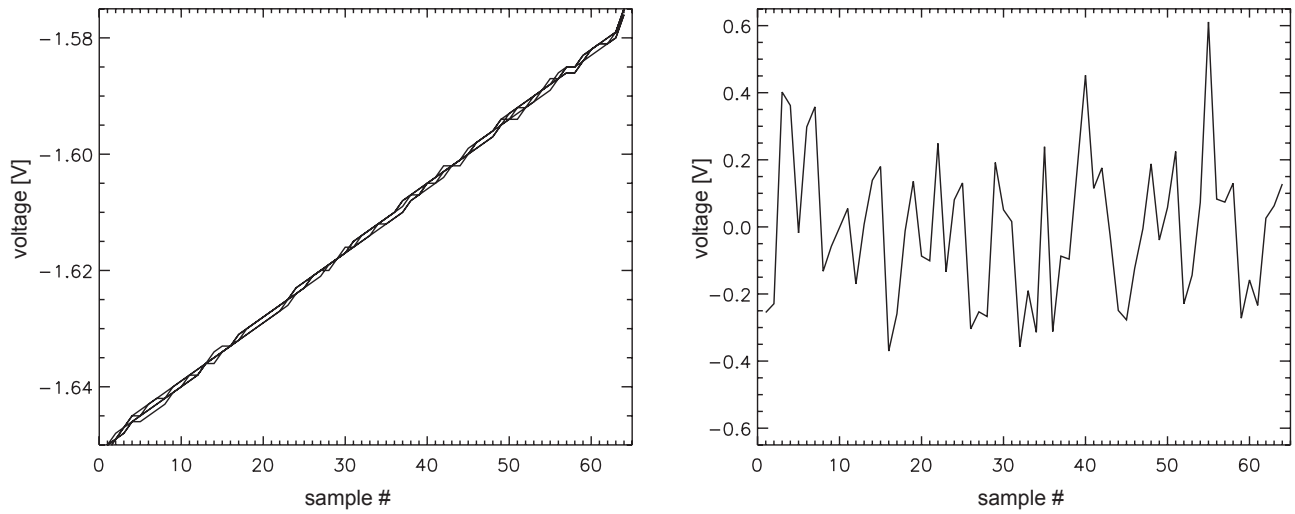

Figure 6. Left: Typical integration ramps measured with a blackbody temperature of 35 K. Right: One of the ramps of the right panel after subtraction of the average ramp slope.

3.2.3. Dark Current

During the first cool downs of the instrument, some of the pixels of the red as well as the blue modules were blocked from incoming light by applying aluminum foil directly at the end of the light cones. The signal measured in this configuration is generated by the dark current of the pixels rather then light leaks in the cryostat shields and baffles. This was confirmed by an independent measurement of the modules in one of the well characterized PACS/Herschel detectors test cryostats. We measured a typical dark current around 1.4×10^5 e^-/s at a bias voltage of 50 mV for the high stress (600-700 N/mm^2) modules, and 5×10^4 e^-/s at 70 mV bias for the low stress ($\sim$100 N/mm^2) modules. The dark current measured for an unstressed PACS module for comparison is around 2500 e^-/s at 200 mV bias. The dark current obviously is a strong function of the applied stress and also depends on the bias voltage and the detector temperature. Below a detector temperature of $\sim$2K no further decrease of the dark current could be observed. The comparatively high dark current found for our pixels are still far lower than the estimated combined background signal from the SOFIA telescope and the optical components of the instrument, which is in the order of $\sim 2 \times 10^7$ e^-/s. The dark current will therefore not degrade the performance of the instrument in any way.

3.3. Diffraction Effects

Due to their size of only 3 $\times$ 15 mm corresponding to 20 wavelengths at 150 μm, the slicer mirrors are cutting significantly into the Airy disk of the telescope (see Fig. 7), causing strong diffraction from that point on. Because of the limited size of the following optical components diffracted light might 'fall off' the mirrors leading to geometrical light loss effects. Detailed modeling of diffraction effects has been performed using the software package GLAD Version 4.5 to estimate the overall throughput of the spectrometer. Detailed results of this analysis for the central slice of the red spectrometer where already presented.[5] In this paper we show new results for off-center slices calculated during the PhD thesis of one of the co-authors.[12]

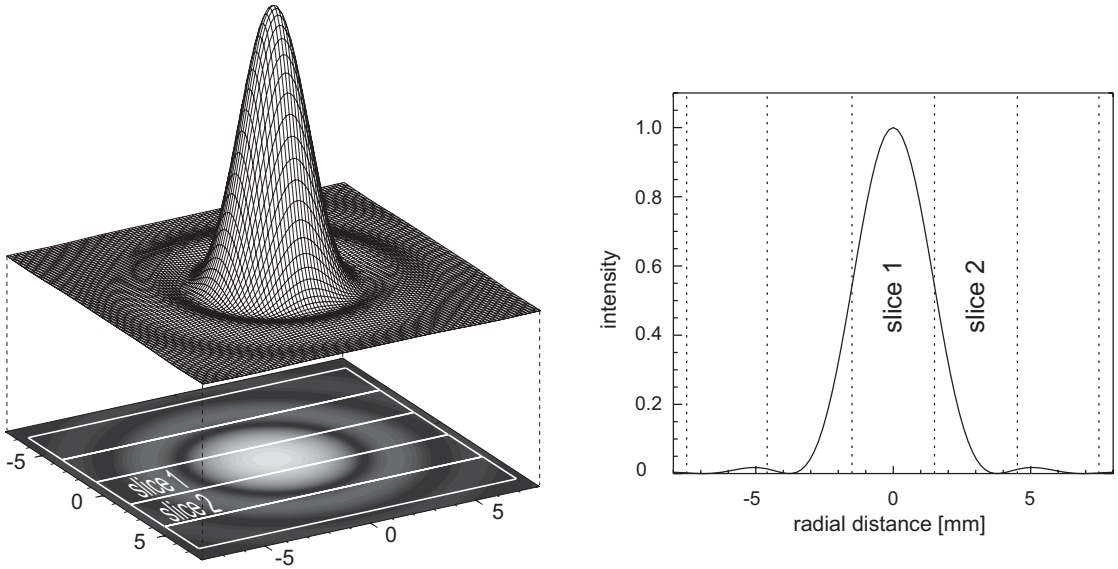

Figure 7. The image of a monochromatic (160 μm) point source at the slicer mirrors of FIFI LS. Left: Three dimensional representation of the diffraction pattern (Airy function) and the projected intensity. The white rectangles represent the individual slicer mirrors and show how the mirrors cut into the Airy disc. Right: The intensity as a function of radial distance. The dotted vertical lines indicate the width of the individual slicer mirrors.

Fig. 8 shows the integrated light loss from diffraction and vignetting after each mirror surface[5,6] in the long wavelength spectrometer for the light falling on the central slice (indicated as slice 1 in Fig. 7) and the first off-axis slice (slice 2 in Fig. 7) respectively. The intensity was normalized to 100% light at the respective slicer

mirror. As the analysis shows, most of the light is lost after the capture mirrors of the slicer assembly and the first few mirrors after the image slicer system (fold mirror and collimator A). The figure also shows that significantly more light is lost on its way through the first off-axis slice than through the central slice. The reason for this effect is that the part of the Airy pattern falling on the first off-axis slice has the highest intensity directly at the edge of this mirror, resulting in more pronounced diffraction effects with more light in the side lobes and consequently more light falling off the following mirrors. The total throughput of the optical system for all the light in the Airy disk is around 80% at most wavelengths. The light loss due to diffraction effects is therefore in the order of the two other major contributions of the overall FIFI LS throughput: The quantum efficiency of the detectors (∼30%) and the grating efficiency (median efficiency ∼70%).

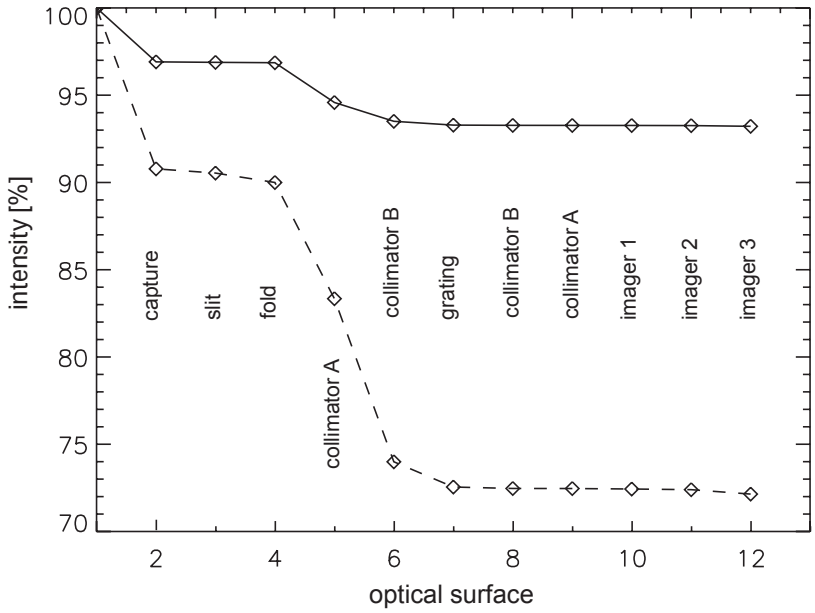

Figure 8. The light loss through the long wavelength spectrometer (for 160 μm) due to diffraction effects and vignetting by the indicated optical surface. The solid line shows the light loss through the central slice, the dashed line through the first off-center slice respectively.

4. CONCLUSION

The integral field spectrometer FIFI LS - being one of the first light instruments on SOFIA - will provide new crucial data for far-infrared astrophysics. The instrument in nearing completion and will be flight ready by end of the year, waiting for completion of the SOFIA observatory. All components of both spectrometer channels have been purchased, delivered, and verified. This includes all optical elements, diffraction gratings, filters, and dichroics. All modules of the high stress and about a third of the low stress detector array are assembled and fully tested. The entire long wavelength spectrometer is assembled and the characterization of the system performance has started. First tests show, that the performance of the instruments will meet our specified requirements.

REFERENCES

1. W. Raab, N. Geis, A. Poglitsch, D. Rosenthal, A. Urban, T. Henning, and J. Beeman, "The Field-Imaging Far-Infrared Line Spectrometer FIFI LS," in *Infrared Spaceborne Remote Sensing VII*, M. Strojnik and B. Andresen, eds., *Proc. SPIE* **3759**, pp. 86–96, 1999.
2. L. Looney, N. Geis, R. Genzel, W. Park, A. Poglitsch, W. Raab, D. Rosenthal, and A. Urban, "Realizing 3D spectral imaging in the far-infrared: FIFI LS," in *Airborne Telescope Systems*, R. Melugin and H. Röser, eds., *Proc. SPIE* **4014**, pp. 14–22, 2000.

3. L. Looney, W. Raab, A. Poglitsch, N. Geis, D. Rosenthal, R. Hönle, R. Klein, F. Fumi, R. Genzel, and T. Henning, "FIFI LS: a Far-Infrared 3D Spectral Imager for SOFIA," in *Airborne Telescope Systems II*, R. Melugin and H. Röser, eds., *Proc. SPIE* **4857**, pp. 47–55, 2002.
4. L. Looney, W. Raab, A. Poglitsch, and N. Geis, "Realizing Integral Field Spectroscopy in the Far-Infrared," *ApJ* **597**, pp. 628–643, 2003.
5. W. Raab, A. P. L. Looney, R. Klein, N. Geis, R. Hönle, W. Viehauser, R. Genzel, M. Hamidouche, T. Henning, and E. Haller, "FIFI LS: the far-infrared integral field spectrometer for SOFIA," in *Ground-based Instrumentation for Astronomy*, A. F. Moorwood and M. Iye, eds., *Proc. SPIE* **5492**, pp. 1074–1085, 2004.
6. R. Klein, A. Poglitsch, W. Raab, N. Geis, M. Hamidouche, R. Hönle, L. Looney, W. Viehauser, R. Genzel, and E. H. T. Henning, "FIFI LS: the far-infrared integral field spectrometer for SOFIA," *Proc. SPIE* **6269**, 2006.
7. D. Rosenthal, J. Beeman, N. Geis, L. Looney, A. Poglitsch, W. Park, W. Raab, and A. Urban, "16×25 Ge:Ga detector arrays for FIFI LS," in *Airborne Telescope Systems*, R. Melugin and H. Röser, eds., *Proc. SPIE* **4014**, pp. 156–163, 2000.
8. A. Poglitsch, R. Katterloher, R. Hönle, J. Beeman, E. Haller, H. Richter, U. Grözinger, N. Haegel, and A. Krabbe, "Far-Infrared Photoconductor Arrays for Herschel and SOFIA," in *Millimeter and Submillimeter Detectors for Astronomy*, T. Phillips and J. Zmuidzinas, eds., *Proc. SPIE* **4855**, pp. 115–128, 2002.
9. R. Hoenle, *PhD thesis*, Ludwig-Maximilians-Universitaet, Muenchen, 2006 (in preparation).
10. Y. Creten, O. Charlier, P. Merken, J. Putzeys, and C. van Hoof, "A 4.2 K readout channel in a standard 0.7 μm CMOS process for a photoconductor array camera," *Journal de Physique IV* **12**, pp. 203–206, 2003.
11. A. Poglitsch, C. Waelkens, and N. Geis, "The Photoconductor Array Camera & Spectrometer (PACS) for the Far Infrared and Submillimetre Telescope (FIRST)," in *UV, Optical, and IR Space Telescopes and Instruments*, J. Breckinridge and P. Jakobsen, eds., *Proc. SPIE* **4013**, pp. 221–232, 2000.
12. W. Viehhauser, *PhD thesis*, Ludwig-Maximilians-Universitaet, Muenchen, 2006 (in preparation).